Multi-spectral palmprint Recognition based on Oriented Multiscale log-Gabor Filters

Meriem Dorsaf Bounneche[a,b], Larbi Boubchir[b,*], Ahmed Bouridane[c], Bachir Nekhoul[a], Arab Ali-Chérif[b]

[a]*LAMEL Lab., University of Jijel, BP 98 Ouled Aissa, Jijel 18000, Algeria*
[b]*LIASD research Lab., Department of Computer Science, University of Paris 8 2 rue de la Liberté 93526 Saint-Denis, France*
[c]*Department of Computer Science and Digital Technologies, University of Northumbria, Newcastle upon Tyne, NE2 1XE, UK*

Abstract

Among several palmprint recognition methods proposed recently, coding-based approaches using multi-spectral palmprint images are attractive owing to their high recognition rates. Aiming to further improve the performance of these approaches, this paper presents a novel multi-spectral palmprint recognition approach based on oriented multiscale log-Gabor filters. The proposed method aims to enhance the recognition performances by proposing novel solutions at three stages of the recognition process. Inspired by the bitwise competitive coding, the feature extraction employs a multi-resolution log-Gabor filtering where the final feature map is composed by the winning codes of the lowest filters' bank response. The matching process employs a bitwise Hamming distance and Kullback-Leibler divergence as novel metrics to enable an efficient capture of the intra- and inter-similarities between palmprint feature maps. Finally, the decision stage is carried pout using a fusion of the scores generated from of different spectral bands to reduce overlapping. In addition, a fusion of the feature maps through two proposed novel feature fusion techniques to allow us to eliminate the inherent redundancy of the features of neighboring spectral bands is also

*Corresponding author
Email addresses: md.alioua@univ-jijel.dz, maya@ai.univ-paris8.fr (Meriem Dorsaf Bounneche), larbi.boubchir@ai.univ-paris8.fr (Larbi Boubchir), ahmed.bouridane@northumbria.ac.uk (Ahmed Bouridane), nek_cem@univ-jijel.dz (Bachir Nekhoul), aa@ai.univ-paris8.fr (Arab Ali-Chérif)

proposed. The experimental results obtained using the multi-spectral palmprint database MS-PolyU have shown that the proposed method achieves high accuracy in mono-spectral and multi-spectral recognition performances for both verification and identification modes; and also outperforms the state-of-the-art methods.

Keywords: Palmprint recognition, multi-spectral biometrics, 2D log-Gabor filter, competitive coding, bitwise Hamming distance, Kullback-Leibler divergence, score level fusion, feature map fusion.

1. Introduction

Biometric security is increasingly becoming an important tool to enhance security and bring greater convenience to services requiring authentication and protection of data. Deploying biometric security using physical or behavioral traits for personal verification and identification [1] is useful in various applications such as forensic science or access control thus resulting in an increase of research interest. Several modalities have been studied and developed including iris, face, gait, key-stroke, finger-print and palmprint [1] where some of them are already well known and widely used depending to the application domain.

The main factors of merits of palmprint images include reliability, stability, user friendliness, non-intrusiveness, flexibility and discriminating ability. These factors arise from a large selection of unique palmprint features including principal lines, wrinkles, ridges, minutiae points and texture. Although, palmprint recognition has been investigated during the last decade, this paper aims to further improve the recognition accuracy, specifically by using multi-spectral imagery that provides more discriminating information in the feature extraction. The multi-spectral palmprint images are collected under different spectra (called also spectral bands) peaking at different light wavelengths. The absorptive and reflective of human skin properties make different wavelengths penetrate the skin layers differently, hence highlight particular features [2].

Various palmprint recognition methods have been proposed recently, and

among them, coding-based approaches using multi-spectral palmprint images are attractive owing to their high recognition rates. In this research work, we propose a novel multi-spectral palmprint recognition approach based on oriented multiscale log-Gabor filters with the aim to further improve the performance of these approaches. The proposed approach enhances the recognition performances by proposing novel techniques at the three stages of a typical biometric cognition process: (i) using bitwise competitive coding, the feature extraction is based on a multi-resolution log-Gabor filtering where the final feature map is composed by the winning codes of the lowest filters' bank real response. (ii) Matching is performed by using the bitwise Hamming distance and the Kullback-Leibler divergence as novel metric to capture efficiently the intra- and inter-spectral similarities between palmprint feature maps, at this stage, we have performed, through two novel features fusion techniques, a fusion of the feature maps in order to eliminate the inherent redundancy of neighboring spectral bands features. (iii) Finally, the decision is carried out either from the obtained fused features similarity scores or from the classic fusion of the scores of different spectral bands aiming reduce overlapping. The experimental results obtained using the multi-spectral palmprint database MS-PolyU have shown that the proposed method achieves high recognition accuracy for mono-spectral and multi-spectral datasets for both verification and identification achieving up to 0.0087 in terms of Equal Error Rate (EER) and 99.77% in terms of highest Identification Rate (IR) at rank-1, respectively. In addition, the proposed method outperforms related state-of-the-art methods especially the similar method proposed in [2] by up to -0.0034 in terms of EER for MS-PolyU database; and also the methods proposed in [2, 3, 4, 5, 6, 7, 8].

The remainder of this paper is as follows: Section 2 depicts related and relevant state-of the-art works. Section 3 describes in detail the proposed methodology including the principle of a multi-spectral palmprint recognition system, the feature extraction, the matching and the fusion strategies while the experiments and results carried out to validate the proposed methodology are given in Section 4. Finally Section 5 concludes the paper.

2. Related works

A crucial step in a typical palmprint recognition system revolves around the feature extraction process which aims to provide and capture the most discriminating information from the extracted Region Of Interest (ROI). To achieve this, several available algorithms can be grouped as follows: structural-based approaches (e.g. minutiae based on SIFT or SURF features, lines based on Sobel/Canny features, and local line directional patterns) [9, 10], appearance-based approaches (e.g. sub space-based on EigenPalm and PCA) [11], statistical-based approaches (e.g., Gabor and Wavelet) [12, 2], coding-based approaches (e.g. phase such as palm-code) [13], and finally hybrid-approaches since they use various techniques (e.g. 2D FLPP) [14, 15].

The success of coding-based methods, which encode the responses of a bank of filters into bitwise features, have attracted our interest, particularly, the multi-scale scheme, where the palm lines can be represented at higher scales. Various algorithms inspired by this approach have been proposed. For example, Zhang et al. proposed an effective Palm-code algorithm in [12] based on a normalized 2D Gabor filter. In [16], Kong et al. presented their competitive coding approach where the dominant orientation is encoded. In [3], Jia et al. proposed the line orientation code based on a modified Finite Radon transform which is similar to the competitive code; while Zuo et al. proposed in [17] a competitive coding using multi-scale oriented 2D log-Gabor filters. Zhang et al. [2] proposed a multi-spectral approach where the features are extracted by competitive coding using six oriented 2D Gabor filters for each spectral band followed by a score fusion at the recognition stage. In [4], the authors presented a joint palmprint and palm-vein verification scheme where the authors fused the features extracted by Gabor and matched filters from palmprint and vein-palm. Zuo et al. proposed in [18] a sparse competitive code based on second derivative of Gaussians with a bank of eighteen multi-scale oriented filters. In [5], Tahmasebi et al. proposed a Rank-Level Fusion for multi-spectral palmprint system using Gabor filter. More recently, based on a hierarchical approach in [19], Hong et al. fused a rough

feature extraction using a block dominant orientation code which is then refined using a block-based histogram of oriented gradients from the different spectral bands. Cui et al. in [20] exploited a bidirectional representation based on pattern classification. On the other hand, Zhang et al. in [21] collected the recent advanced research works on multi-spectral Biometrics including multi-spectral palmprint recognition. In [22] Xu et al. proposed a novel multispectral palmprint recognition method based jointly on multiclass projection extreme learning machine and digital Shearlet transform. Fei et al. proposed in [7] a palmprint recognition method based on a double half-orientation where a bank of half-Gabor filters are defined for the half-orientation extraction. Another palmprint recognition method was proposed in [8] using a double-orientation code based on Gabor filters and nonlinear matching scheme. The proposed methods in [7, 8] have been assessed on multi-spectral palmprint MS-PolyU database.

Competitive coding is the association of a filtering process which exploits neurophysiology-based Gabor function to capture the discriminative orientation information with a competitive rule: winner-takes-all using the palm line contrast. It is a state-of-the-art texture-based feature extraction algorithm widely used and is inspired from human vision's system [16] which tends to compare palm lines as a method/tool to compare palm images. These lines: (i) are specific multi-scale features since the principal ones are robust and well represented at large scales whereas wrinkles at smaller ones may appear or disappear with changes of lighting, (ii) can be categorized as *positive* when they are bright or as *negative* when they are dark [23].

In the spatial domain, a 2D Gabor function is a Gaussian multiplied by a complex exponential and can be seen as a Gaussian shifted from the origin in the Fourier domain. Its mathematical properties such as the smooth infinitely differentiable shape, the monomodal modulus and the highly joint localization in space, orientation and frequency make it a good choice for various image processing applications. In addition, 2D Gabor function can be used as a model which follows as much as possible the neuroscience knowledge on the simple cells receptive field's properties of the Primary Visual Cortex (V1) of primates

on the statistics of natural images [24].

However, this function has a few drawbacks: (i) non-orthogonality which implies non-invertibility witch is not really a problem in our feature extraction use, (ii) its deficiency to cover uniformly the mid frequencies as it is a bandpass filter, (iii) its bad coverage of low and high frequencies due to an excessive overlapping, and (iv) the non-zero DC component which increases as the bandwidth is widened resulting from the tails' overlapping of the sum of two Gaussians centered at plus and minus the central frequency.

It is worth noting that natural images are better encoded using filters having transfer functions which are Gaussian viewed on the logarithmic frequency scale [25]. Therefore, a log-Gabor can be a better alternative to the Gabor filtering since its transfer function is viewed on the logarithmic frequency scale including the constraint of the maximum bandwidth which limited to approximately one octave on Gabor filters which is not optimal if one is seeking a broader spectral information with maximal spatial localization. Therefore, that log-Gabor filters can offer attractive power especially in image feature discrimination.

In this paper, we have chosen a multi-resolution approach which is justified by the properties of the palmprint lines discussed previously and by a physiological basis claiming that, for each location of a palmprint image, there are cells that cover at least three scales over a minimum of four octaves [26] in addition of an improved principal line's representation at large scales.

Finally, our proposed approach aims to improve the efficiency of the competitive coding for palmprint recognition by using a multi-resolution log-Gabor feature extraction scheme. This is achieved by proposing and combining two matching processes on the same feature to enhance the generated matching scores using a new fusion scheme of the different spectrum features.

3. Proposed methodology

This section describes the proposed multi-spectral palmprint recognition process, feature extraction, coding and matching processes including the fusion

strategy at the score and feature levels. The multi-resolution log-Gabor filter is employed at the feature extraction stage to extract an indexed feature map based on the competitive rule and encoded in Gray binary code as listed in Table 1 where the matching score between the final feature maps is computed using bitwise Hamming distance and Kullback-Leibler (KL) divergence on each spectral band of the multi-spectral database used. In other words, this score fusion is proposed to enhance the mono-spectral accuracy. Finally new feature's map fusions are proposed to further evaluate and appreciate the multi-spectral discriminating efficiency.

3.1. Multi-spectral palmprint recognition process

The multi-spectral palmprint recognition system is illustrated in Figure 1 where the user's palms are captured under four different lights: Red, Blue, Green and Near Infra Red denoted NIR. The corresponding ROIs are extracted as shown in Figure 2. A feature extraction is then carried out of the ROIs to compute the resulting set of features which are stored in a reference database at the enrollment step. At the recognition stage, the same procedure is used to extract the set of features of a given user and matched against the features from the reference database. A similarity score is finally employed so that a decision of accepting or rejecting the requested user is made.

3.2. Feature extraction

Competitive code uses the orientation and type of line information based on Gabor filters and winner-takes-all rule. It operates as follows: the argument of the minimum real intensity value of the filtered image pixels (in the same spatial position) among the six filtered images is considered to be the pixel's value in the processed image [16].

The proposed feature extraction scheme is inspired and based on the competitive orientation coding where the dominant orientations of the multi-resolution (scales and orientations) log-Gabor coefficients are encoded. We propose to

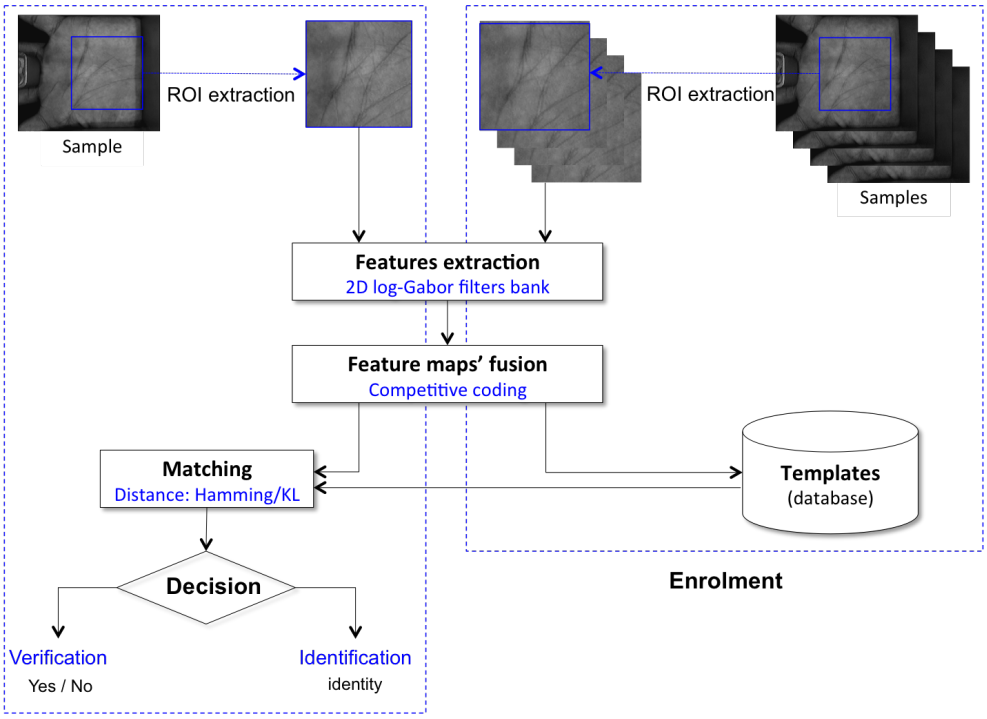

Figure 1: Multi-spectral palmprint recognition process flow diagram.

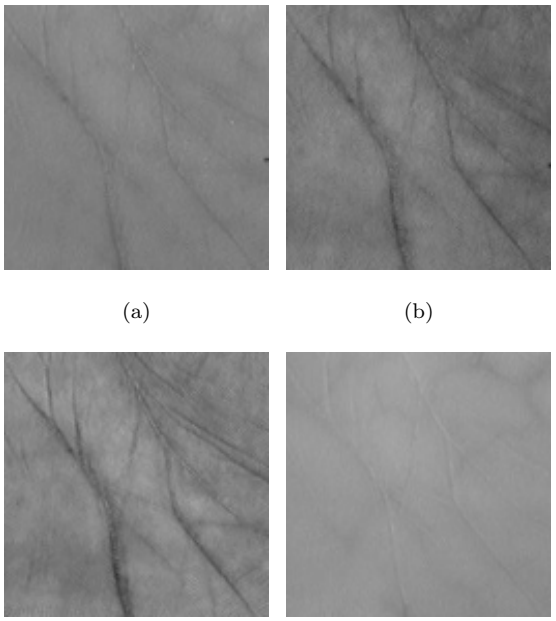

Figure 2: ROI images of a palmprint multi-spectral image under four different spectral bands: (a) Red, (b) Green, (c) Blue and (d) NIR.

use a multi-resolution log-Gabor filter which strengthens the excellent mathematical properties of Gabor filters aiming to make some improvements so that the highest frequency bands would be covered by narrowly localized oriented filters while the set of filters would cover uniformly the Fourier domain including the highest and lowest frequencies. Such improved characteristics should make the transform a more promising tool for the processing of natural images. To achieve this, a bank of 24 log-Gabor filters are applied on each palm image along four scales and six orientations in the range of $[0^o, 180^o]$ (i.e., $\{0, \pi/6, \pi/3, \pi/2, 2\pi/3, 5\pi/6\}$); where the indexes (s, o) of each element corresponding to the lowest real intensity value of pixels (in the same spatial position) among the 24 filtered images will serve to compute its new value in the indexed image [16].

The log-Gabor filter bank frequency response is given by:

$$LG_{(f_0,\theta_0)}(\rho,\theta) = \exp\left(-\frac{[\log(\rho/f_0)]^2}{2{\sigma_\rho}^2}\right).\exp\left(-\frac{(\theta-\theta_0)^2}{2{\sigma_\theta}^2}\right) \quad (1)$$

where (ρ, θ) represents the polar coordinates, f_0 is the center frequency of the filter, θ_0 is the orientation angle of the filter, σ_ρ determines the scale bandwidth and σ_θ indicates the angular bandwidth.

Figure 3 illustrates the filtered images along four scales and six orientations obtained using the bank of 24 log-Gabor filters applied on a ROI image under the Green spectral band.

The winner scale and orientation indexes for each element from the filtered images, denoted $\binom{s}{o}$, can be computed as:

$$\binom{s}{o} = \arg\min_{s,o}\left(I(x,y) * lg_{(f_s,\theta_o)}(x,y)\right) \quad (2)$$

where I is the palm image, $lg_{(f_s,\theta_o)}$ is the spatial filter response at scale s and orientation o. (x, y) represents the spatial location of each element and $*$ is the convolution product.

Therefore, the feature vector of each palm contains a five bit code of the winer indexes at each element as listed in Table 1 allowing us to make a bitwise

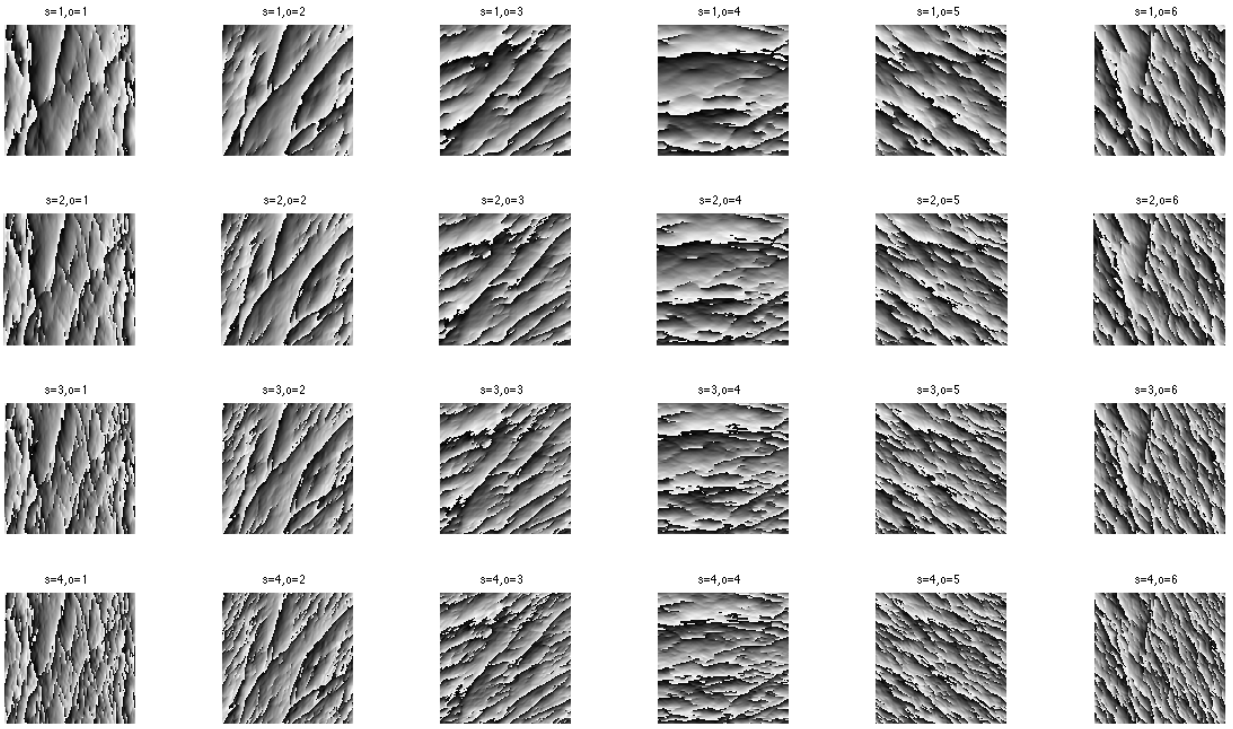

Figure 3: An example of filtered images along four scales and six orientations obtained using the bank of 24 log-Gabor filters applied on a ROI image under Green spectral band.

representation of the corresponding 24 states (4 scales and 6 orientations) of the multi-resolution filters indexes [16].

Figure 4 shows the feature maps extracted from the ROI images in Figure 2. The different gray values represent different orientation features.

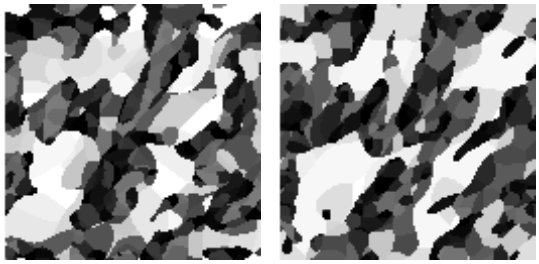

(a) Red (b) Green

(c) Blue (d) NIR

Figure 4: Feature maps extracted from the ROI images in Figure 2.

3.3. Matching process

The matching process as follows: given two palm features with one stored in the template (gallery set)and the second from the probe set, a similarity score is measured to check whether the features are extracted from the same palm or not. Therefore this subsection will deal with two similarity measures used in the matching process. First, a bitwise Hamming distance is used so that our results can be compared against those of Zhang et al. [2]. Second, KL divergence metric is adapted and used to further improve the recognition rates. The best scores for both methods were measured by taking care of reducing the translation's

Table 1: Bit representation of the multi-resolution coding based on Gray binary code. *The Gray binary code is used to code the 24 states corresponding to the scale and orientation indexes. For example, the first binary code 00000 is used to code the orientation 0 at scale 1, and the last binary code 11100 is used to code the orientation $5\pi/6$ at scale 4.*

Scale	Orientation	State	Bit 0	Bit 1	Bit 2	Bit 3	Bit 4
1	0	1	0	0	0	0	0
	$\pi/6$	2	0	0	0	0	1
	$\pi/3$	3	0	0	0	1	1
	$\pi/2$	4	0	0	0	1	0
	$2\pi/3$	5	0	0	1	1	0
	$5\pi/6$	6	0	0	1	1	1
2	0	7	0	0	1	0	1
	$\pi/6$	8	0	0	1	0	0
	$\pi/3$	9	0	1	1	0	0
	$\pi/2$	10	0	1	1	0	1
	$2\pi/3$	11	0	1	1	1	1
	$5\pi/6$	12	0	1	1	1	0
3	0	13	0	1	0	1	0
	$\pi/6$	14	0	1	0	1	1
	$\pi/3$	15	0	1	0	0	1
	$\pi/2$	16	0	1	0	0	0
	$2\pi/3$	17	1	1	0	0	0
	$5\pi/6$	18	1	1	0	0	1
4	0	19	1	1	0	1	1
	$\pi/6$	20	1	1	0	1	0
	$\pi/3$	21	1	1	1	1	0
	$\pi/2$	22	1	1	1	1	1
	$2\pi/3$	23	1	1	1	0	1
	$5\pi/6$	24	1	1	1	0	0

effect in ROI extraction process. Hence, the test map was translated from -3 to 3 both vertically and horizontally and a distance is computed between the same template and those obtained by any translation where the minimum value is chosen as the best and most similar one.

3.3.1. Hamming distance

Hamming distance is the sum of a basic XOR logic operations between the two maps normalized to values lying between 0 and 1 so that a distance value of 0 represents a perfect match while a value of 1 represents a perfect difference. The normalized bitwise Hamming distance is given by:

$$D_{Hamm}(P,Q) = \frac{\sum_{y=0}^{M-1}\sum_{x=0}^{N-1}\sum_{i=1}^{5}(P_i^b(x,y) \bigotimes Q_i^b(x,y))}{5NM} \tag{3}$$

where P and Q are the stored and the tested multi-resolution palmprint feature maps, respectively. P_i^b and Q_i^b are their i^{th} bit plane. N and M are the size of the palmprint image and (x, y) indicates the element's location, respectively.

3.3.2. Kullback-Leibler divergence

The KL divergence is a frequently used information-theoretic distance metric [27, 28]. It is computed from the expected P and the observed Q intensity distributions. In our case, these probability distributions are replaced by the multi-resolution feature maps. The KL divergence between the two maps is given by:

$$d_{KL}(P,Q) = \sum_{j=0}^{(M-1)(N-1)}\sum_{i=1}^{5} P_i(j)\log\left(\frac{P_i(j)}{Q_i(j)}\right) \tag{4}$$

where $P_i(.)$ and $Q_i(.)$ are the vectors of size $(1 \times MN)$ of the stored and tested multi-resolution palmprint feature maps P and Q, respectively.

The major properties of d_{KL} [27, 28] are: (1) its values are strictly positive if the observed and expected maps are not equal (i.e., $P \neq Q$), (2) on the other hand, the value of d_{KL} is equal to 0 if the maps are exactly similar.

In this study, a normalization of D_{KL} is performed to allow a comparison of

two distances as follows:

$$D_{KL}(P,Q) = \frac{d_{KL}(P,Q) - \min(d_{KL}(P,Q))}{\max(d_{KL}(P,Q)) - \min(d_{KL}(P,Q))} \quad (5)$$

where D_{KL} is the normalized distance. $\min(d_{KL})$ and $\max(d_{KL})$ are the minimum and the maximum of the non-normalized d_{KL}, respectively.

3.4. Inter-spectral and Intra-spectral analysis

The use of multi-spectral database aims to enhance the recognition rates versus mono spectral counterpart by adding more discriminative information content to the feature vectors. However, this comes at the expense of inherently adding more redundancy which can be counter-productive if not dealt with appropriately. A quantitative study of this inter-spectral correlation has been carried out on the palmprint extracted feature maps. Therefore, a log-Gabor mono-spectral feature extraction is performed and the inter-spectral distances using bitwise Hamming and KL distances in (3) and (5) are calculated for the same palm.

Table 2 summarizes the inter-spectral distances statistics whereas Table 3 shows the intra-spectral counterparts. The majors finding from these statistical analysis are: (1) when using D_{Hamm} the inter-spectral feature maps distance is proportional to inter-bands color light wavelengths witch supports the theory that each spectrum can highlight its specific feature space. (2) The most significant inter-spectral distance observed remains lower than intra-spectral one when using D_{Hamm} while D_{KL} provides some inter-spectral distances that can be close to imposter means especially for the distances between Blue and NIR and that between Green and NIR. This strengthens the analysis of highlighting unique characteristics under each spectrum. (3) The D_{KL} distance between Blue and Green and between Red and NIR are very low thus demonstrating that the correlation between them is very important, hence their fusion would not be efficient. (4) The D_{KL} values reflect more quantitatively different palms than D_{Hamm}.

Table 2: Inter-spectral band distances statistics using the proposed methods with the state-of-the-art method in [2].

Spectral band	Method	Distance statistics	Red	Green	Blue	NIR
Red	Gabor+D_{Hamm} (Zhang et al. [2])	D_{mean}	0	0.3030	0.3110	0.2566
		D_{min}	0	0.2002	0.2083	0.1523
		D_{max}	0	0.4486	0.4420	0.3828
	log-Gabor+D_{Hamm} (Proposed method)	D_{mean}	0	0.4238	0.4113	0.2835
		D_{min}	0	0.3666	0.3620	0.1701
		D_{max}	0	0.4871	0.4674	0.4639
	log-Gabor+D_{KL} (Proposed method)	D_{mean}	0	0.0787	0.1062	0.0119
		D_{min}	0	0	0	0
		D_{max}	0	0.5119	0.5493	0.6025
Green	Gabor+D_{Hamm} (Zhang et al. [2])	D_{mean}		0	0.1571	0.3840
		D_{min}		0	0.0915	0.2920
		D_{max}		0	0.3441	0.4650
	log-Gabor+D_{Hamm} (Proposed method)	D_{mean}		0	0.2472	0.4566
		D_{min}		0	0.1351	0.4016
		D_{max}		0	0.3958	0.5083
	log-Gabor+D_{KL} (Proposed method)	D_{mean}		0	0.0107	0.2797
		D_{min}		0	0	0
		D_{max}		0	0.3625	0.7637
Blue	Gabor+D_{Hamm} (Zhang et al. [2])	D_{mean}			0	0.3910
		D_{min}			0	0.2884
		D_{max}			0	0.4801
	log-Gabor+D_{Hamm} (Proposed method)	D_{mean}			0	0.4494
		D_{min}			0	0.3901
		D_{max}			0	0.5078
	log-Gabor+D_{KL} (Proposed method)	D_{mean}			0	0.3213
		D_{min}			0	0
		D_{max}			0	0.8794

Table 3: Intra-spectral band distances statistics using the proposed methods with the state-of-the-art method in [2].

Spectral band	Genuine mean			Imposter mean		
	Gabor+D_{Hamm} Zhang et al. [2]	log-Gabor+D_{Hamm} (proposed method)	log-Gabor+D_{KL} (proposed method)	Gabor+D_{Hamm} Zhang et al. [2]	log-Gabor+D_{Hamm} (proposed method)	log-Gabor+D_{KL} (proposed method)
Blue	0.2600	0.2599	0.1290	0.4621	0.4508	0.7681
Green	0.2686	0.2887	0.1376	0.4686	0.4686	0.7693
Red	0.2143	0.2542	0.1338	0.4561	0.4514	0.7632
NIR	0.2511	0.2554	0.1406	0.4627	0.4533	0.7611

3.5. Fusion schemes

Despite the redundancy factor, a multi-spectral analysis is used to enhance the system performances. Therefore, several fusion schemes were proposed to achieve this goal while still keeping the added information captured from the multi-spectral analysis. Although, fusion can be performed at different levels of the recognition process, we have chosen to deploy two fusion methods: at the score and the feature maps levels. In the first one, the distances are computed on each spectral band and four different schemes are developed: (i) a basic mean of the four mono-spectral scores, (ii) a weighed by the reciprocal of Equal Error Rate (1/EER) mean of the four mono-spectral scores [29], (iii) a basic mean of new normalized scores, and (iv) a weighted by (1/EER) means of new normalized scores already weighted by the combination of overlapping percentage as proposed in [2] to reduce correlation effects.

The *basic mean* distance, denoted d_m, is defined as:

$$d_m(P,Q) = \frac{1}{k}\sum_{i=1}^{k} D(\mathcal{M}_i^P, \mathcal{M}_i^Q) \tag{6}$$

where $\mathcal{M}_i^P$ and $\mathcal{M}_i^Q$ are the palmprint feature maps of P and Q, respectively, at i^{th} kind/band, and k is the total number of kinds. D is Hamming or KL distance.

We can also define the *weighted mean* distance, denoted d_{wm}, as:

$$d_{wm}(P,Q) = \sum_{i=1}^{k} w_i D(\mathcal{M}_i^P, \mathcal{M}_i^Q) \tag{7}$$

where

$$w_i = \frac{(1/\sum_{i=1}^{k} \frac{1}{EER_i})}{EER_i} \tag{8}$$

The two last fused scores are computed using both equations (6) and (7) but with a new normalized distance $D^{'} = W_{overlap}D$ proposed in [2] (equations (5) and (6) in [2] or their adapted scheme to the four spectral bands used to calculate $d^{'}$) where $W_{overlap}$ is a combination of different spectral band overlapping percentages.

The second method is concerned with two fusion strategies of the extracted feature maps fusions which are combined to eliminate redundancy resulting from similar features which exist among different spectral bands. The first method is inspired by the technique proposed in [2] where it was observed that summing the inter-spectral scores may make the process fail because of overlapping. The idea was then to reduce the redundancy by eliminating all redundant feature elements having similar values over different feature maps. For example, if we perform a Hamming distance of two feature maps belonging to the same spectral band on two different spectra, the two obtained maps would get rid of the similarities over each spectral band but fusing these maps by summing them would sometimes lead to a misclassification due to redundancy. For this is reason, our fused scores would be better implemented using logic AND between the resulting XORed maps. This would ensure that two feature elements having the same value in different spectral bands will be zero'ed Ii.e., eliminated) after the XOR and will not be considered in the last fused score.

Let us consider two types of feature maps $\mathcal{M}_i^P$ where $i = 1, 2$ for two samples $\{P, Q\}$. The fused score, denoted as $D_{\wedge}^{(MF)}$, would be:

$$D_{\wedge}^{(MF)} = \frac{1}{MN} \sum_{x=0}^{M-1} \sum_{y=0}^{N-1} D(\mathcal{M}_1^P(x,y), \mathcal{M}_1^Q(x,y)) \wedge D(\mathcal{M}_2^P(x,y), \mathcal{M}_2^Q(x,y)) \tag{9}$$

where $\wedge$ is the AND logical operator and D is the distance used.

The second feature maps fusion method is concerned with a scheme based on logic and arithmetic operators aiming to reduce the overlapping effect in the

fused feature maps. The idea is similar to the previous one, but a notion of inter-spectral difference between two bands' maps was considered in this case. Therefore, it makes sense to employ logic operators when dealing with Hamming distance to deal with binary values. In addition, an inter-spectral distance is added to the scheme used above. However, the arithmetic operations were applied for KL divergence having real values. An example of the fusion of two bands' maps is given by equations (8) and (9) for Hamming and KL distances, respectively:

$$\begin{aligned} D_{\wedge Hamm}^{(MF)} = \frac{1}{5MN} \sum_{x=0}^{M-1} \sum_{y=0}^{N-1} [D_{Hamm}(\mathcal{M}_1^P(x,y), \mathcal{M}_1^Q(x,y)) \\ \wedge D_{Hamm}(\mathcal{M}_2^P(x,y), \mathcal{M}_2^Q(x,y))] \\ \wedge D_{Hamm}(\mathcal{M}_1^P(x,y), \mathcal{M}_2^P(x,y)) \end{aligned} \tag{10}$$

where $\wedge$ is the AND logical operator.

$$\begin{aligned} D_{\wedge KL}^{(MF)} = \sum_{j=0}^{(M-1)(N-1)} \frac{1}{2} [D_{KL}(\mathcal{M}_1^P(j), \mathcal{M}_1^Q(j)) \\ + D_{KL}(\mathcal{M}_2^P(j), \mathcal{M}_2^Q(j))] \\ - \frac{1}{2} [D_{KL}(\mathcal{M}_1^P(j), \mathcal{M}_2^P(j)) + D_{KL}(\mathcal{M}_1^Q(j), \mathcal{M}_2^Q(j))] \end{aligned} \tag{11}$$

where $\mathcal{M}$ is the vector of size $(1 \times MN)$ of the feature map. The second part of the two equations above represents the difference between spectrums.

4. Experimental results, analysis and discussion

In these experiments, we have evaluated the performance of the proposed palmprint recognition approach using the multi-spectral palmprint MS-PolyU database described in Section 4.1. Experimental results obtained for both verification and identification modes are analyzed and discussed in Section 4.2 and 4.3, respectively. These results are obtained for the mono-spectral and multi-spectral cases including the use of the proposed fusion techniques described in

Section 3.5. In addition, the results are also compared against the state-of-the-art methods in order to demonstrate the effectiveness of our proposed method. Section 4.4 discusses and analyzes the speed performance of our method.

4.1. Multi-spectral database

The multi-spectral palmprint MS-PolyU database described in [30] consists of palmprint images collected from 250 persons (195 males and 55 females) having an age range between 20 and 60 years. The palmprint images were collected in two separate sessions where in each one 6 images of each hand were provided by each subject under 4 different illuminations producing 24 samples of each palm of an individual. The database contains 6000 images from 500 different palmprints for each illumination. The two sessions were separated by about 9 days. The four illuminations cover three spectral bands in the visible spectrum where the peaking wavelength for Blue, Green and Red were $470nm$, $525nm$ and $660nm$, respectively. The last band, NIR, is peaking at $880nm$.

The ROI multi-spectral database contains also the ROIs extracted from the multi-spectral palmprints database. Each ROI is a square sub image of a fixed size: 128×128 represented in a coordinate system and extracted by the algorithm described in [12].

4.2. Mono-spectral verification and identification

The inter-spectral analysis shows that each spectral band can highlight its discriminative information to enhance the overall system recognition accuracy, thus suggesting that each spectrum should have its own parameters to provide the best segregated feature maps. This section aims to investigate and determine these parameters to obtain the lowest EER and the highest accuracy (ACC) corresponding to the threshold of EER where the False Rejection Rate (FRR) is equal to False Acceptance Rate (FAR), for the verification, the highest IR at rank-1 for the identification on each band. We note here that EER is computed in the range of [0,1] where IR and ACC are computed in terms of '%'.

The best combination of the four filter parameters is investigated, i.e., the center frequency f_0, scale bandwidth σ_ρ, the angular bandwidth σ_θ, and the scaling factor between the successive filters. Our choice of both bandwidths σ_ρ and σ_θ was inspired by [31] where the purpose was to be as close as possible to the physiological knowledge of simple cortical cells which are known to be organized in quadrature pairs of phase strengthening the complex filter values.

The database was divided into a *Gallery* set containing the palmprints provided in the first section and a *Test* set holding those of the second section. Each feature map from the test set was matched with all the maps in the gallery set using both distances in (3) and (4). A genuine match is obtained if both feature maps emanate from the same palm while it will be considered as imposter if the maps are provided from two different palms. For the verification and identification modes, the EER and the IR rank-1 are used to evaluate the system performance. There are 18000 genuine ($6 \times 500 \times 6$) among 9000000 total matches. More than fifty parameters combinations were tried for each spectral band and the best results are reported in Table 4 and compared against the results described in [2]. From the results obtained, it can be seen, first, that our proposed method using KL distance (namely log-Gabor+D_{KL} in the table) outperforms the state-of-the-art method in [2] (namely Gabor+D_{Hamm}) in terms of EER for all spectral bands. Moreover, our second proposed method using bitwise Hamming distance (namely log-Gabor+D_{Hamm}) also outperforms the method in [2] for the three spectrums: Green, Blue and NIR. Furthermore, this method achieves performances slightly below than the performances of [2] for the Red spectrum but they remain comparable. This is confirmed in terms of ACC where the best results are in the range of $[97.17\%, 98.41\%]$. The ACC results were obtained at the threshold where both acceptance and rejection errors are equal.

Table 5 shows the identification results based on IR at rank-1 of the proposed methods for each spectral band. From the results it can be noticed that the method using bitwise Hamming distance slightly outperforms the method using KL distance for the four spectral bands, but still remains comparable.

Table 4: Mono-spectral verification results of the proposed methods with the state-of-the-art method in [2] across each spectral band.

Methods	Criteria	Blue	Green	Red	NIR
Gabor+D_{Hamm} [2]	EER	0.0520	0.0575	**0.0212**	0.0398
log-Gabor+D_{Hamm} (proposed method)	EER	**0.0273**	**0.0246**	0.0226	**0.0283**
	ACC	97.27	97.54	97.74	97.17
	Threshold	0.5935	0.5689	0.5921	0.5896
log-Gabor+D_{KL} (proposed method)	EER	**0.0159**	**0.0192**	**0.0212**	**0.0274**
	ACC	98.41	98.08	97.88	97.26
	Threshold	0.4423	0.4196	0.4182	0.4111

Table 5: Mono-spectral identification results of the proposed methods across each spectral band.

Proposed methods	Criteria	Blue	Green	Red	NIR
log-Gabor+D_{Hamm}	IR rank-1	99.23	99.10	99.30	99.33
log-Gabor+D_{KL}	IR rank-1	99.03	98.90	99.13	98.93

4.3. Multi-spectral verification and identification

The fusion approaches described in Section 3.5 were analyzed in terms of their performances to improve the recognition of the mono-spectral palmprint recognition. Table 6 depicts the verification matching results obtained using the conventional fusion techniques based on the score level approach and the proposed fusion methods based on feature maps. The proposed methods, log-Gabor+D_{Hamm} and log-Gabor+D_{KL} in the table, were compared against the state-of-the-art method in [2] (e.g., Gabor+D_{Hamm}) for all possible combinations of spectral bands using the fusion methods described previously. By analyzing these results, it can be noticed that, firstly, our proposed methods outperform the method in [2] for most spectral bands combinations using the conventional fusion techniques based on score level (i.e. d_m, $d_m^{'}$, d_{wm} and $d_{wm}^{'}$) except for the following spectral bands combination: Red-Blue, Red-NIR, Red-Blue-NIR; where the method in [2] surpasses the proposed methods for at least three conventional fusion techniques. Secondly, the method 'log-Gabor+D_{KL}' outperforms the method 'Gabor+D_{Hamm}' in terms of EER in almost all cases. This indicates that the use of KL distance has allowed us to improve the recognition performance when compared against the bitwise Hamming distance. Furthermore, the 'log-Gabor+D_{KL}' method with the proposed fusion method $D_{\wedge}^{(MF)}$ achieves the lowest EERs in the range of $[0.0087, 0.0133]$ for all spectral band combinations except only for Red-NIR combination where the best EER is obtained for the method in [2] and also 'log-Gabor+D_{Hamm}' method using the fusion metric $d_m^{'}$. Moreover, the use of the proposed fusion approach using $D_{\wedge}^{(MF)}$ with 'log-Gabor+D_{KL}' method achieves the best results in terms of EER compared against log-Gabor+D_{Hamm}' method. This confirms once again that the use of KL distance is able to improve the recognition performances compared to the use of Hamming distance. In addition, the proposed fusion method using $D_{\wedge}^{(MF)}$ achieves better results in terms of EER compared to the second proposed fusion method using $D_{\wedge Hamm}^{(MF)}$ or $D_{\wedge KL}^{(MF)}$. This is due to the considerable overlapping removal using $D_{\wedge Hamm}^{(MF)}$ or $D_{\wedge KL}^{(MF)}$ which resulted in a decrease of discriminative properties. Finally, the best result corresponding to the lowest

Table 6: Multi-spectral verification results of the proposed methods with the state-of-the-art method in [2] for different fusion methods across different spectral band combinations. *The results are given for all possible combinations of the spectral bands using the fusion techniques discussed in Section 3.5. The first four fusion techniques are the state-of-the-art score fusion schemes and the two last ones are our proposed feature fusion methods. The results are given in terms of EER.*

Fusion methods	d_m	d'_m	d_{wm}	d'_{wm}	$D_{\wedge}^{(MF)}$ (proposed method 1)	$D_{\wedge Hamm}^{(MF)}/D_{\wedge KL}^{(MF)}$ (proposed method 2)
Blue & Green						
Gabor+D_{Hamm} [2]	0.0425	0.0425	0.0397	0.0397/	/	/
log-Gabor+D_{Hamm}	0.0228	0.0141	0.0238	0.0146	0.0209	0.0464
log-Gabor+D_{kL}	0.0137	0.0137	0.0145	0.0145	**0.0133**	0.0335
Blue & Red						
Gabor+D_{Hamm} [2]	0.0154	0.0154	0.0121	0.0121	/	/
log-Gabor+D_{Hamm}	0.0166	0.0124	0.0174	0.0134	0.0127	0.0144
log-Gabor+D_{kL}	0.0122	0.0122	0.0135	0.0135	**0.0107**	0.0148
Blue & NIR						
Gabor+D_{Hamm} [2]	0.0212	0.0212	0.0212	0.0212	/	/
log-Gabor+D_{Hamm}	0.0150	0.0119	0.0162	0.0124	0.0117	0.0106
log-Gabor+D_{kL}	0.0119	0.0119	0.0129	0.0129	**0.0094**	0.0135
Green & Red						
Gabor+D_{Hamm} [2]	0.0212	0.0212	0.0182	0.0182	/	/
log-Gabor+D_{Hamm}	0.0157	0.0114	0.0173	0.0126	0.0115	0.0152
log-Gabor+D_{kL}	0.0123	0.0123	0.0137	0.0135	**0.0112**	0.0139
Green & NIR						
Gabor+D_{Hamm} [2]	0.0242	0.0242	0.0181	0.0181	/	/
log-Gabor+D_{Hamm}	0.0157	0.0114	0.0170	0.0132	0.0125	0.0132
log-Gabor+D_{kL}	0.0122	0.0122	0.0143	0.0143	**0.0109**	0.0143
Red & NIR						
Gabor+D_{Hamm} [2]	**0.0152**	**0.0152**	**0.0152**	**0.0152**	/	/
log-Gabor+D_{Hamm}	0.0203	**0.0153**	0.0205	0.0161	0.0183	0.0418
log-Gabor+D_{kL}	0.0172	0.0172	0.0180	0.0180	0.0164	0.0283
Blue & Green & Red						
Gabor+D_{Hamm} [2]	0.0243	0.0212	0.0152	0.0151	/	/
log-Gabor+D_{Hamm}	0.0167	0.0110	0.0174	0.0120	0.0154	0.0134
log-Gabor+D_{kL}	0.0110	0.0110	0.0125	0.0125	**0.0091**	0.0154
Blue & Green & NIR						
Gabor+D_{Hamm} [2]	0.0212	0.0214	0.0212	0.0212	/	/
log-Gabor+D_{Hamm}	0.0142	0.0105	0.0166	0.0119	0.0129	0.0110
log-Gabor+D_{kL}	0.0102	0.0102	0.0119	0.0119	**0.0092**	0.0131
Blue & Red & NIR						
Gabor+D_{Hamm} [2]	0.0121	0.0121	0.0121	0.0121	/	/
log-Gabor+D_{Hamm}	0.0143	0.0112	0.0156	0.0126	0.0128	0.0104
log-Gabor+D_{kL}	0.0115	0.0115	0.0129	0.0129	**0.0096**	0.0136
Green & Red & NIR						
Gabor+D_{Hamm} [2]	0.0153	0.0156	0.0152	0.0150	/	/
log-Gabor+D_{Hamm}	0.0139	0.0117	0.0160	0.0127	0.0140	0.0113
log-Gabor+D_{kL}	0.0119	0.0119	0.0137	0.0137	**0.0103**	0.0139
Blue & Green & Red & NIR						
Gabor+D_{Hamm} [2]	0.0152	0.0151	0.0121	0.0121	/	/
log-Gabor+D_{Hamm}	0.0135	0.0104	0.0153	0.0114	0.0154	0.0105
log-Gabor+D_{kL}	0.0099	0.0099	0.0118	0.0120	**0.0087**	0.0118

ERR of 0.0087 was obtained using log-Gabor+D_{KL} method with the first feature maps fusion rule $D_{\wedge}^{(MF)}$ for Blue-Green-Red-NIR combination. Compared the state-of-the-art method in [2] where the best EER is 0.0121 obtained using the score fusion scheme to reduce overlapping, our proposed approach offers significantly better performance.

The Receiver Operating Characteristic (ROC) curves for different spectral bands are shown in Figure 5 where the best results for the verification mode is obtained using KL divergence for each spectral band and also for their fusion are illustrated. The fusion result is obtained using $D_{\wedge}^{(MF)}$ corresponding to the combination of the four spectral bands. From the results, it can be seen that the fusion results outperform those obtained for each spectral band separately. This confirms that the proposed fusion technique has allowed us to improve significantly the authentication performances of the mono-spectral palmprint recognition system.

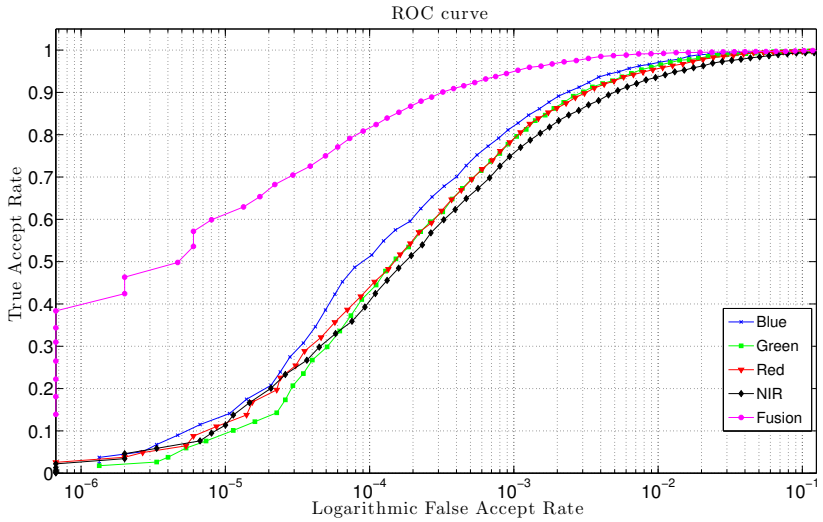

Figure 5: ROC curves of the proposed method based on KL distance for each spectral band and for the fusion of all spectral bands.

We have also compared our proposed approach based on oriented multiscale

log-Gabor filters against the state-of-the-art methods. Table VII shows the best verification results obtained versus the results from the following state-of-the-art methods: (i) palmprint verification method based on line orientation code in [3], (ii) a joint palmprint and palm-vein recognition method based on Gabor filter in [4], (iii) multi-spectral palmprint recognition method based on Gabor filter using rank-level fusion in [5], (iv) multi-spectral palmprint recognition method based on Gabor filter using competitive code with score-level fusion in [2], (v) palmprint recognition method using the extended binary orientation co-occurrence vector coding [6], (vi) palmprint recognition method based on double half-orientation using a bank of half-Gabor filters, and (vii) palmprint recognition method based on Gabor filter using a double-orientation code with nonlinear matching scheme [8]. Table 7 shows the best verification results of these methods obtained using PolyU and MS-PolyU palmprint databases. From the results obtained, it can be noticed that our method based on 2D log-Gabor with KL distance achieves a lower EER compared against the rest of the state-of-the-art counterparts (i.e. [2, 3, 4, 5, 7, 8]). In addition, our second method based on 2D log-Gabor with bitwise Hamming distance outperforms the Zhang's method based on Gabor filter with bitwise Hamming distance in [4]. This is due to the deployment of log-Gabor filter which integrates both scale and orientation information compared to a conventional Gabor filter.

Furthermore, we have assessed the identification performances of the proposed methods. Table 8 illustrates the identification results in terms of IR at rank-1 for different fusion techniques across different spectral band combinations. It can be seen that the fusion approaches have improved the identification rates at rank-1 than mono-spectral identification (see results in Table 5) with a best IR at rank-1 of 99.77% obtained for the combined spectral bands: Blue-Green-Red-NIR, using 'log-Gabor+D_{KL}' method with the second fusion approach of feature maps (i.e., $D_{\wedge KL}^{(MF)}$). In addition, the proposed methods, 'log-Gabor+D_{Hamm}' and 'log-Gabor+D_{KL}' achieve similar identification performances.

Figure 6 shows the Cumulative Match Curves (CMC) depicting only the

Table 7: Comparing the best verification performance of the proposed methods with the state-of-the-art methods.

Method	Feature extraction	Distance	Database	Spectral band	EER
Jia et al. (2008) [3]	Finite Radon transform	Pixel to area match	PolyU	/	0.1600
Zhang et al. (2011) [4]	Gabor filter+Competitive coding	Bitwise Hamming	MS-PolyU	NIR	0.0158
	Gaussian filter+ binarization	Bitwise AND & OR	PolyU	/	
Tahmasebi et al. (2011) [5]	Concatenated 2D Gabor filter	Hamming	MS-PolyU	Blue–Green–Red–NIR	0.0143
Zhang et al. (2010) [2]	Gabor filter+Competitive coding	Bitwise Hamming	MS-PolyU	Blue–Red	0.0121
Zhang et al. (2012) [6]	Extended binary orientation	Bitwise Hamming	PolyU	/	0.0316
	co-occurrence vector		MSPolyU	blue	0.0225
Fei et al. (2016) [7]	Half Gabor filter	Bitwise Hamming	PolyU	/	0.0204
	+Double Half Orientation Code		MSPolyU	red	0.0131
Fei et al. (2016) [8]	Gabor filter+Double competitive coding	Nonlinear angular match	PolyU	/	0.0092
			MSPolyU	red	0.0119
Proposed method 1	2D log-Gabor filter+competitive coding	Bitwise Hamming	MS-PolyU	Blue–Red–NIR	0.0104
Proposed method 2	2D log-Gabor filter+competitive coding	Kullback-Leibler	MS-PolyU	Blue–Green–Red–NIR	**0.0087**

best results of the proposed methods. We can see that the result of the fusion obtained using KL distance is higher than the results obtained for each spectral band using bitwise Hamming distance. Once again, this confirms that the proposed fusion technique has enabled us to improve significantly the identification performances of our proposed recognition system.

4.4. Speed performance

The proposed method was implemented using MATLAB R2014a on a MacBook Pro with OS X El Capitan, Intel Core i7 CPU (2.8 GHz) and 16 GB RAM. The execution time for feature extraction and feature matching steps is listed in Table 9 and compared with the state-of-the-art method in [2]. By analyzing the execution times (average time over 50 runs), both steps in our method (i.e. feature extraction and feature matching) have execution times slightly superior to those in [2] but remains less than 1 second (between [0.8943,0.9279] second). Also, the feature matching step is fast compared to feature extraction step. This suggests that our proposed method can be integrated in an offline or online system of multi-spectral palmprint verification. Furthermore, this execution time

Table 8: Multi-spectral identification results of the proposed methods for different fusion techniques across different spectral bands combinations. The results shown related the IR at rank-1.

Proposed methods	Fusion methods					
	d_m	d'_m	d_{wm}	d'_{wm}	$D_{\wedge}^{(MF)}$	$D_{\wedge Hamm}^{(MF)}/D_{\wedge KL}^{(MF)}$
Blue & Green						
log-Gabor+D_{Hamm}	**99.33**	**99.33**	**99.33**	**99.33**	98.77	76.50
log-Gabor+D_{KL}	99.20	99.20	99.20	99.20	**99.30**	**96.20**
Blue & Red						
log-Gabor+D_{Hamm}	99.43	99.43	99.43	99.43	99.33	99.30
log-Gabor+D_{KL}	**99.57**	**99.57**	**99.50**	**99.50**	**99.43**	**99.53**
Blue & NIR						
log-Gabor+D_{Hamm}	**99.63**	99.60	**99.63**	**99.60**	**99.63**	99.57
log-Gabor+D_{KL}	**99.63**	**99.63**	99.60	**99.60**	**99.63**	**99.73**
Green & Red						
log-Gabor+D_{Hamm}	**99.53**	**99.53**	99.47	99.47	99.40	**99.43**
log-Gabor+D_{KL}L	**99.53**	**99.53**	**99.50**	**99.50**	**99.43**	99.37
Green & NIR						
log-Gabor+D_{Hamm}	**99.67**	**99.67**	**99.67**	**99.67**	**99.67**	99.57
log-Gabor+D_{KL}	99.60	99.60	99.63	99.63	**99.67**	**99.60**
Red & NIR						
log-Gabor+D_{Hamm}	**99.47**	**99.50**	**99.50**	**99.50**	99.57	92.33
log-Gabor+D_{KL}	**99.47**	99.47	99.47	99.47	**99.67**	**98.63**
Blue & Green & Red						
log-Gabor+D_{Hamm}	**99.57**	**99.57**	99.57	99.57	99.27	**99.27**
log-Gabor+D_{KL}	**99.57**	**99.57**	**99.60**	**99.60**	**99.47**	**99.27**
Blue & Green & NIR						
log-Gabor+D_{Hamm}	**99.63**	**99.67**	**99.67**	**99.67**	99.33	**99.57**
log-Gabor+D_{KL}	**99.63**	99.63	99.63	99.63	**99.57**	**99.57**
Blue & Red & NIR						
log-Gabor+D_{Hamm}	99.63	99.63	99.63	99.60	**99.63**	99.57
log-Gabor+D_{KL}	**99.67**	**99.67**	**99.67**	**99.67**	**99.63**	**99.77**
Green & Red & NIR						
log-Gabor+D_{Hamm}	**99.67**	**99.63**	99.60	99.60	99.60	99.63
log-Gabor+D_{KL}	99.63	**99.63**	**99.67**	**99.67**	**99.63**	**99.70**
Blue & Green & Red & NIR						
log-Gabor+D_{Hamm}	99.63	99.63	99.60	99.60	99.33	99.50
log-Gabor+D_{KL}	**99.67**	**99.67**	**99.63**	**99.67**	**99.63**	**99.77**

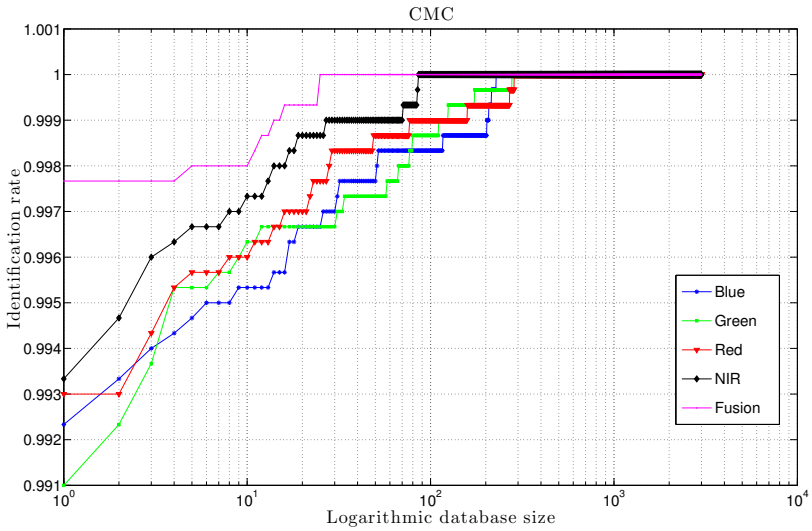

Figure 6: CMC curves of the proposed method based on bitwise Hamming distance for each spectral band and also for the fusion of all spectral bands.

is acceptable and enough to design a real-time application. It is to be noted that the run times were obtained from a simple implementation without any effort to optimize the implementation. This suggests that it is possible to further reduce the computational time by optimizing the program code.

5. Conclusion

This paper has discussed a new multi-specral palmprint recognition approach based on oriented multi-scale log-Gabor filters and bitwise competitive coding. We have also proposed a novel matching process that employs the bitwise Hamming distance and the KL divergence allowing us to capture efficiently the similarities between palmprint feature maps generated using 2D log-Gabor filters with bitwise competitive code. Secondly, we have proposed two fusion techniques of feature maps for matching step in order to to eliminate the inherent redundancy of features of neighbouring spectral bands. The experimental results on MS-PolyU database have shown that the proposed approach achieves

Table 9: Execution time of the proposed method compared with the state-of-the-art method [2]. *The execution time (average time over 50 runs) of feature extraction step is given for the four spectral bands. The execution time for feature matching step in our method is given for the two proposed fusion techniques based on Hamming distance and KL divergence using six training images of the template.*

	Execution time (seconds)	
	Proposed method	Zhang et al. [2]
Step 1 : Feature extraction	0.2235×4	0.0197×4
Step 2 : Feature matching		
(1) based on score level fusion scheme		
- using bitwise Hamming distance	$0.0815\ .\ 10^{-3} \times 4$	$(0.0561\ .\ 10^{-3}) \times 4$
- using proposed KL distance	0.0014×4	/
(2) based on feature map fusion scheme		
- proposed fusion method 1 (with Hamming)	0.0057	/
- proposed fusion method 1 (with KL)	0.0173	/
- proposed fusion method 2 (with Hamming)	0.0073	/
- proposed fusion method 2 (with KL)	0.0339	/

improved mono-spectral and multi-spectral performances for both verification and identification modes. The proposed technique also outperforms the state-of-the-art methods, in particular, the method in [2]. Our future work is to focus on improvement of the feature extraction by studying the different oriented multi-scale representations [32] with a view to be able to further capture the discriminative information of the orientations in addition to the scales.

6. References

[1] A.K. Jain, A. Ross and K. Nandakuma, *Introduction to Biometric*, Springer, ISBN 978-0-387-77325-4, 2011.

[2] D. Zhang, Z. Guo, G. Lu, L. Zhang and W. Zuo, *An Online System of multi-spectral palmprint Verification*, IEEE Transactions on Instrumentation and Measurement, vol. 59(2), pp. 480–490, 2010.

[3] W. Jia, D. -S. Huang and D. Zhang, *Palmprint verification based on robust line orientation code*, Pattern Recognition, vol. 41(5), pp. 1504–1513, 2008.

[4] D. Zhang, Z. Guo, G. Lu, L. Zhang, Y. Liu and W. Zuo, *Online joint palmprint and palm-vein verification*, Expert Systems with Applications, vol. 38(3), pp. 2621–2631, 2011.

[5] A. Tahmasebi, H. Pourghasem and H. M. Nasab, *A Novel Rank-Level Fusion for multi-spectral palmprint Identification System*, International Conference on Intelligent Computation and Bio-Medical Instrumentation (ICBMI), pp. 208–211, 2011.

[6] L. Zhang, H. Li and J. Niu, *Fragile Bits in Palmprint Recognition*, IEEE Signal Processing Letters, vol. 19(10), pp. 663–666, 2012.

[7] L. Fei, Y. Xu and D. Zhang, *Half-orientation extraction of palmprint features*, Pattern Recognition Letters, vol. 69, pp. 35–41, 2016.

[8] L. Fei, Y. Xu, W. Tang and D. Zhang, *Double-orientation code and nonlinear matching scheme for palmprint recognition*, Pattern Recognition, vol. 49, pp. 89–101, 2016.

[9] G. S. Badrinath and P. Gupta, *Palmprint Verification using SIFT features*, First Workshops on Image Processing Theory, Tools and Applications (IPTA), pp. 1–8, 2008.

[10] Y. Luo, L. Zhao, B. Zhang, W. Jia, F. Xue, J. Lu, Y. Zhu and B. Xu, *Local line directional pattern for palmprint recognition*, Pattern Recognition, vol. 50, pp. 26–44, 2016.

[11] S. Ribaric and I. Fratric, *A biometric identification system based on eigenpalm and eigenfinger features*, IEEE Transactions on Pattern Analysis and Machine Intelligence, vol. 27(11), pp. 1698–1709, 2005.

[12] D. Zhang, W. Kong, J. You and M. Wong, *Online palmprint identification*, IEEE Transactions on Pattern Analysis and Machine Intelligence, vol. 25(9), pp. 1041–1050, 2003.

[13] A. Kumar and H. C. Shen, *Palmprint Identification using PalmCodes*, Third International Conference on Image and Graphics (ICIG), pp. 258–261, 2004.

[14] M. Laadjel, A. Bouridane, F. Kurugollu, O. Nibouche and W. Q Yan, *Partial palmprint Matching Using Invariant Local Minutiae Descriptors*, Transactions on Data Hiding and Multimedia Security V, Volume 6010 of the series LNCS, pp. 1–17, 2010.

[15] M. Laadjel, A. Bouridane, O. Nibouche, F. Kurugollu and S. Al-Maadeed, *An improved palmprint recognition system using iris features*, Journal of Real-Time Image Processing, vol. 8(3), pp. 253–263, 2013.

[16] A. W. -K. Kong and D. Zhang, *Competitive Coding Scheme for palmprint Verification*, The 17*th* International Conference on Pattern Recognition (ICPR), vol. 1, pp. 520–523, 2004.

[17] W. Zuo, F. Yue, K. Wang and D. Zhang, *Multiscale Competitive Code for Efficient palmprint Recognition*, The 19^{th} International Conference on Pattern Recognition (ICPR), pp. 1–4, 2008.

[18] W. Zuo, Z. Lin, Z. Guo and D. Zhang, *The Multiscale Competitive Code via Sparse Representation for Palmprint Verification*, IEEE Conference on Computer Vision and Pattern Recognition (CVPR), pp. 2265–2272, 2010.

[19] D. Hong, W. Liu, J. Su, Z. Pan and G. Wang, *A novel hierarchical approach for multi-spectral palmprint recognition*, Neurocomputing, vol. 151, part 1, pp. 511–521, 2015.

[20] J. Cui, J. Wen and Z. Fan, *Appearance-based bidirectional representation for palmprint recognition*, Multimedia Tools and Applications, vol. 74(24), pp. 10989–11001, 2015.

[21] D. Zhang, Z. Guo and Y. Gong, *Multispectral Biometrics: Systems and Applications*, Springer, ISBN 978-3-319-22485-5, 2015.

[22] X. Xu, L. Lu, X. Zhang, H. Lu and W. Deng, *Multispectral palmprint recognition using multiclass projection extreme learning machine and digital shearlet transform*, Extreme Learning Machine And Applications, Neural Computing and Applications, vol. 27(1), pp. 143–153, 2016.

[23] J. Rodrigues and J. M. Hans du Buf, *Visual Cortex Frontend: Integrating Lines, Edges, Keypoints, and Disparity*, Image Analysis and Recognition, Volume 3211 of the series LNCS, pp. 664–671, 2004.

[24] J. G. Daugman, *Uncertainty relation for resolution in space, spatial frequency, and orientation optimized by two-dimensional visual cortical filters*, Journal of the Optical Society of America A, vol. 2(7), pp. 1160–1169, 1985.

[25] D. J. Field, *Relations between the statistics of natural images and the response properties of cortical cells*, Journal of the Optical Society of America A, vol. 4(12), pp. 2379–2394, 1987.

[26] R. L. De Valois, D. G. Albrecht and L. G.Thorell, *Spatial frequency selectivity of cells in macaque visual cortex*, Vision Research, vol. 22(5), pp. 545–559, 1982.

[27] S. Kullback and R. Leibler, *On information and sufficiency*, Annals of Mathematical Statistics, vol. 22,? pp. 79–86, 1951.

[28] A. C. S. Chung, W. M. Wells, A. Norbash and W. E. L. Grimson, *Multimodal Image Registration by Minimising Kullback-Leibler Distance*, International Conference on Medical Image Computing and Computer Assisted Intervention (MICCAI), vol. 2489 of the series LNCS, pp. 525–532, 2002.

[29] R. Snelick, U. Uludag, A. Mink, M. Indovina and A. Jain, *Large-Scale Evaluation of Multimodal Biometric Authentication Using State-of-the-art Systems*, IEEE Transactions on Pattern Analysis and Machine Intelligence, vol. 27(3), pp. 450–455, 2005.

[30] PolyU multi-spectral palmprint database, *http://www4.comp.polyu.edu.hk/~biometrics/MultispectralPalmprint/MSP.htm*.

[31] S. Fischer, F. Sroubek, L. Perrinet, R. Redondo and G. Cristobal, *Self-Invertible 2D log-Gabor Wavelets*, International Journal of Computer Vision, vol. 75(2), pp. 231–246, 2007.

[32] L. Boubchir, A. Nait-Ali and E. Petit, *Multivariate statistical modeling of images in sparse multiscale transforms domain*, The 17^{th} IEEE International Conference on Image Processing (ICIP), pp. 1877-1880, 2010.